Available online at www.sciencedirect.com
ScienceDirect
Journal of Power Sources 173 (2007) 291–297
JOURNAL OF POWER SOURCES
www.elsevier.com/locate/jpowsour

Reducibility of $Ce_{1-x}Gd_xO_{2-\delta}$ in prospective working conditions

D. Pérez-Coll [a], D. Marrero-López [a], J.C. Ruiz-Morales [a], P. Núñez [a,*], J.C.C. Abrantes [b], J.R. Frade [c]

[a] Dep. de Química Inorgánica, Universidad de La Laguna, E-38200 La Laguna, Tenerife, Spain
[b] ESTG, Instituto Politécnico de Viana do Castelo, 4900 Viana do Castelo, Portugal
[c] Dep. Engenharia Cerâmica e do Vidrio, CICECO Universidade de Aveiro, 3810-193 Aveiro, Portugal

Received 26 December 2006; received in revised form 4 April 2007; accepted 29 April 2007
Available online 5 May 2007

Abstract

Nanocrystalline powders of CGO materials with different contents of Gd were prepared by a freeze-drying method and used to prepare dense ceramic samples. This method allowed one to obtain good quality samples to re-examine the reducibility of CGO materials. These materials were characterized by a combination of coulometric titration, impedance spectroscopy and ion blocking measurements to evaluate changes in point defect chemistry and mixed conducting properties. We have examined the onset of n-type conductivity as a function of temperature and oxygen partial pressure, and this information was used to re-examine the mixed transport properties in reducing conditions imposed by fuels, and also the OCV obtained with CGO solid electrolyte cells under air/CGO/fuel gradients. The polaron mobility was also evaluated and was found to depend slightly on temperature and to decrease with increasing oxygen deficiency. This confirmed that the electronic conductivity is mainly dependent on reducibility.

Keywords: Gadolinium doped ceria; Ion blocking; Coulometric titration; Electronic conductivity; Reducing conditions

1. Introduction

Ceria materials with rare earth additives (Y^{3+}, Gd^{3+}, Sm^{3+}, La^{3+}...) are potential electrolyte materials for intermediate temperature applications [1–6], except possibly for the onset of n-type electronic conductivity. The decrease in the oxygen partial pressure increases the non-stoichiometry accompanied by partial reduction of Ce^{4+} to Ce^{3+}, causing the onset of electronic conductivity [7–10]. In addition, excessive oxygen stoichiometry changes might spoil the thermo-mechanical stability of ceria-based materials due to stresses imposed by relatively large Ce^{3+} cations. One must thus seek electrolyte compositions with oxygen stoichiometry determined mainly by the content of aliovalent additive and minimum additional changes under reducing conditions.

Nevertheless, enhanced electronic conductivity might be interesting if one considers the use of ceria-based materials as a component of composite or cermet fuel electrodes, such as anodes for solid oxide fuel cells [11–13]. The hypothesis of using ceria materials both as solid electrolyte and component of fuel electrode depends mainly on the limits of electrolytic domain, often taken as the conditions when the ionic transport number is less 0.99.

Though the reducibility might depend on the type of aliovalent additive and its content, the relevant literature includes contradicting data on the non-stoichiometry changes as well as the electronic conductivity. For example, some references suggest that the increase in the trivalent dopant concentration increases the reducibility of ceria-based materials [14–16], and this was also supported by some theoretical simulations [17]. However, other authors showed the opposite trend, i.e., lower changes in oxygen stoichiometry with increase in dopant content [5,18,19]. Usually the electronic conductivity is extracted from the dependence of total conductivity on oxygen partial pressure, under the assumption that the ionic conductivity remains sufficiently smaller than the electronic contribution [20–21]. However, in reducing conditions the increase in oxygen deficiency could lead to both changes in electronic and

* Corresponding author. Tel.: +34 922 318501; fax: +34 922 318461.
E-mail address: pnunez@ull.es (P. Núñez).

0378-7753/$ – see front matter © 2007 Elsevier B.V. All rights reserved.
doi:10.1016/j.jpowsour.2007.04.060

ionic conductivity [22] hindering the separation of ionic and electronic contributions from the total conductivity. Thus, it is appropriate to use alternative techniques to obtain independent measurements of electronic contribution. Hebb–Wagner ion-blocking methods [23,24] have been used in ceria based materials [10,25–30].

One should also re-examine the conclusion that introduction of about 20% of different trivalent cations produces small changes on the electronic conductivity [31], and extend the analysis to wider ranges of composition. In a previous work [32] one analyzed the electronic transport properties of $Ce_{0.8}Sm_{0.2}O_{2-\delta}$ under reducing conditions by independent measurements of the stoichiometric loss and the electronic conductivity. The actual work has now been extended to $Ce_{1-x}Gd_xO_{2-\delta}$, with different fractions x, to assess the effects of composition on reducibility of CGO and transport properties.

2. Experimental

Gd-doped ceria solid solutions $Ce_{1-x}Gd_xO_{2-\delta}$ (x = 0, 0.1, 0.2, 0.3) were prepared by freeze-drying [32,33], using nitrates $Ce(NO_3)_3 \cdot 6H_2O$ (Aldrich, 99.99%) and $Gd(NO_3)_3 \cdot 6H_2O$ (Aldrich, 99.9%). The freeze-dried precursors were calcined at 375 °C for 4 h to decompose nitrates, and XRD patterns confirmed formation of fluorite single phase.

The powders were calcined at 600 °C for 4 h to attain a similar starting condition to perform coulometric titration measurements [34,35] using the experimental systems described elsewhere [32]. The powder is introduced in a Pt crucible and inserted into the electrochemical cell, which comprises a section of YSZ tube and two sealed YSZ pellets to obtain gas tight conditions. Symmetrical Pt electrodes were painted in the internal and external faces of the tube and were connected by Pt wires to a dc power source (Yokogawa 7651), with the interior under cathodic polarization. In this situation, the YSZ tube works as an oxygen pump to extract oxygen thus lowering the oxygen partial pressure inside the cell and reducing the sample. The upper YSZ pellets was adapted to work as an oxygen probe by painting Pt electrodes attached to Pt wires, and using a multichannel multimeter (Keithley 2700 + 7700) for the emf measurements (V_0). According to the Nernst equation:

$$V_0 = \frac{RT}{4F} \ln\left[\frac{pO_2^{\mathrm{ref}}}{pO_2}\right] \quad (1)$$

where R is the universal constant, T absolute temperature, F Faraday constant, and pO_2 and pO_2^{ref} are the inside and outside oxygen partial pressures, respectively (e.g., $pO_2^{\mathrm{ref}} = 0.21$ atm). Every coulometric titration experiment was performed by applying a step change in applied potential to the oxygen pump and using the Faraday law to extract the oxygen stoichiometry change ($\Delta\delta$) from the time dependence of supplied current, i.e.,

$$\Delta\delta = \frac{M_{\mathrm{CGO}}}{m} \frac{1}{2F} \int_{t_1}^{t_2} (I(t) - I_\infty)\,\mathrm{d}t \quad (2)$$

where M_{CGO} is the formula weigth of CGO; m the mass of the sample; t_1 and t_2 are the initial and final times, respectively; I the current through the electrochemical pump, and I_∞ is the residual current at the final steady state conditions. The oxygen sensor was used to monitor transient changes in oxygen partial pressure and to record the steady state value. The changes of oxygen content in the gas phase (inside the cell) were subtracted from the total value of pumped oxygen, to determine the stoichiometric loss of the sample. The voltage supplied to the pump was changed by 50 mV steps with a sequence of increasing values.

The n-type electronic conductivity was measured by Hebb–Wagner/ion blocking technique [10,23–30]. Dense Gd-doped ceria pellets, obtained after sintering at 1600 °C during 10 h were sealed by a ceramic glass against an alumina impervious pellet avoiding oxygen leaks. Pt electrodes were previously painted on both sides of the sample and attached to Pt wires connected to a dc power source (Yokogawa 7651). The inner electrode was polarized cathodically under a given value of applied voltage, until steady state conditions were reached. Transient changes and the steady state value of potential difference across the sample (V_0) were monitorized by a dc multimeter (Keithley 2700 + 7700) using a different pairs of Pt wires connected to the sample electrodes. The sequence of experiments was performed with 50 mV steps, in increasing order, and for the temperature range of 700–1000 °C. The average electronic conductivity for the conditions across the sample can thus be obtained as:

$$\sigma_{\mathrm{e,av}} = \frac{L}{A} \frac{I_{\mathrm{e}}}{V_0} \quad (3)$$

where I_{e} is the electronic current, L the sample thickness and A is the area of the Pt electrodes. This corresponds to the average electronic conductivity under a chemical potential difference across the sample, i.e., air/CGO/pO_2, where pO_2 is obtained from the value of applied voltage (Eq. (1)). Similarly, the electronic conductivity at a fixed value of pO_2 (i.e., without gradient of chemical potential) can be obtained on differentiating the steady state current versus voltage difference across the sample:

$$\sigma_{\mathrm{e}} = \frac{L}{A} \frac{\mathrm{d}I_{\mathrm{e}}}{\mathrm{d}V_0} \quad (4)$$

The ionic conductivity of the sintered pellets was obtained by impedance spectroscopy (Solartron 1260).

3. Reducibility

Fig. 1 shows a typical example of time dependence of current $I(t)$ and emf reading $V_0(t)$ in the coulometric titration cell, after a step change in applied potential (V_{ap}). Numerical integration of current during the transient regime (Eq. (2)) yields the oxygen loss and stoichiometric change of the sample, for the overall change in sensor readings between the start and end of the transient regime. The corresponding dependence of oxygen stoichiometry versus oxygen partial pressure inside the cell is shown in Fig. 2; this reveals sharp rise of reduction at low values of oxygen partial pressure, which is enhanced with increasing temperatures.

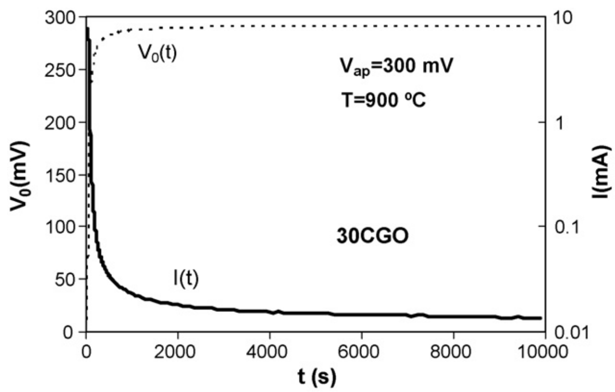

Fig. 1. Time dependence of current (thick line) and voltage (dashed line) in the coulometric titration cell between two equilibrium states, after applying a generic voltage of 300 mV by the dc source.

Fig. 2 shows that the oxygen loss clearly decreases when introducing Gd^{3+} into the CeO_2 host and also decreases when the content of Gd^{3+} increases. This suggests that the presence of the trivalent additive decreases reducibility under prospective working conditions. In order to assess the composition effects one must thus take into account the expected effects of Gd^{3+} on the nominal concentration of oxygen vacancies:

$$\mathrm{Gd_2O_3} \xrightarrow{\mathrm{CeO_2}} 2\mathrm{Gd}'_{\mathrm{Ce}} + V_{\mathrm{O}}^{\bullet\bullet} + 3\mathrm{O}_{\mathrm{O}}^{x} \tag{5}$$

and the reaction of reduction of Ce^{4+} to Ce^{3+} according to:

$$\mathrm{O}_{\mathrm{O}}^{x} + 2\mathrm{Ce}_{\mathrm{Ce}}^{x} \Leftrightarrow \frac{1}{2}\mathrm{O}_2\,(\mathrm{gas}) + V_{\mathrm{O}}^{\bullet\bullet} + 2\mathrm{Ce}'_{\mathrm{Ce}} \tag{6}$$

The corresponding mass action constant can be combined with the electroneutrality condition and other mass and lattice position restrictions, for a more detailed quantitative analysis. On neglecting defect interactions and thus assuming nearly ideal behaviour:

$$K_R = \frac{[V_{\mathrm{O}}^{\bullet\bullet}][\mathrm{Ce}'_{\mathrm{Ce}}]^2 p\mathrm{O}_2^{1/2}}{[\mathrm{O}_{\mathrm{O}}^{x}][\mathrm{Ce}_{\mathrm{Ce}}^{x}]^2} \tag{7}$$

and

$$2[V_{\mathrm{O}}^{\bullet\bullet}] = [\mathrm{Ce}'_{\mathrm{Ce}}] + [\mathrm{Gd}'_{\mathrm{Ce}}] \tag{8}$$

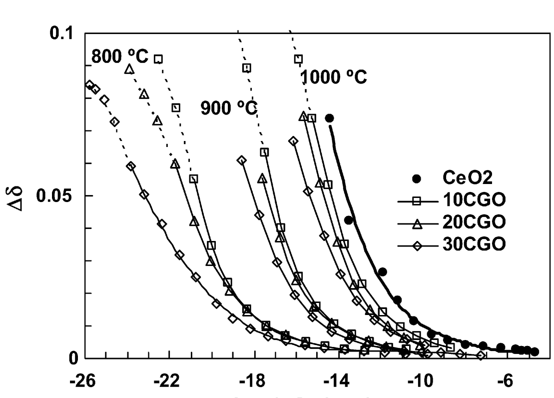

Fig. 2. Dependence of oxygen deficiency $\Delta\delta$ in ceria ($CeO_{2-\Delta\delta}$) and $Ce_{1-x}Gd_xO_{2-x/2-\Delta\delta}$ samples vs. oxygen partial pressure.

with the following relations between the concentrations of relevant species, stoichiometric changes ($\Delta\delta$), and fraction of trivalent additive (x):

$$[\mathrm{Ce}'_{\mathrm{Ce}}] = \frac{8}{v_0}\Delta\delta \tag{9}$$

$$[V_{\mathrm{O}}^{\bullet\bullet}] = \frac{4}{v_0}\left(\Delta\delta + \frac{x}{2}\right) \tag{10}$$

$$[\mathrm{Ce}_{\mathrm{Ce}}^{x}] = \frac{4}{v_0}(1 - x - 2\Delta\delta) \tag{11}$$

$$[\mathrm{O}_{\mathrm{O}}^{X}] = \frac{4}{v_0}\left(2 - \frac{x}{2} - \Delta\delta\right) \tag{12}$$

where v_0 is the unit cell volume. Substitution in Eq. (6) should thus allow one to obtain the values of mass action constant from the entire range of values of $\Delta\delta$ versus pO_2 at a given temperature T:

$$K_R(T) = \frac{4\Delta\delta^2(\Delta\delta + x/2)p\mathrm{O}_2^{1/2}}{(2 - x/2 - \Delta\delta)(1 - x - 2\Delta\delta)^2} \tag{13}$$

We can thus extract the enthalpy of reduction ΔH_R from plots of $\ln(K_R) = (\Delta S_R/R) - (\Delta H_R/R)T^{-1}$, as suggested for CSO [32]. Alternatively, we can extract the enthalpy from the temperature dependence of pO_2. Note that $(pO_2)^{1/2}$ is proportional to K_R at constant oxygen stoichiometry, and thus

$$\ln(p\mathrm{O}_2) = \mathrm{Const} - \frac{2\Delta H_R}{R}T^{-1} \tag{14}$$

The results shown in Fig. 3 correspond to a typical hipo-stoichiometry $\Delta\delta = 0.05$, for CeO_2 (closed circles) and $Ce_{1-x}Gd_xO_{2-x/2-\Delta\delta}$ with $x = 0.1$ (closed squares), $x = 0.2$ (triangles) and $x = 0.3$ (diamonds) and also $\Delta\delta = 0.02$ for $x = 0.1$ (open squares). From the values of slope we have estimated typical values of enthalpy ΔH_R in the range 410–430 kJ/mol. Table 1 shows a comparison between these values and other results reported in the literature.

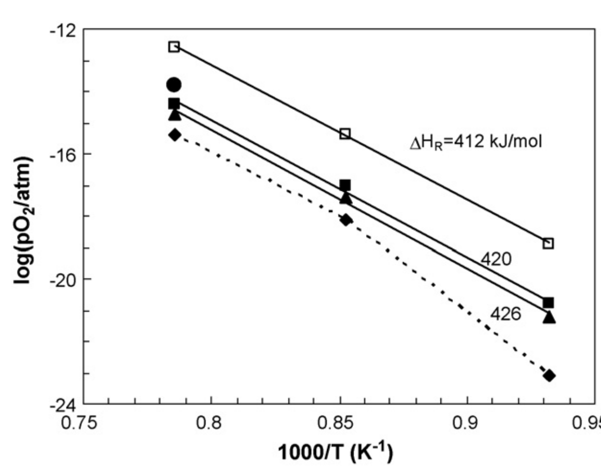

Fig. 3. Temperature dependence of oxygen partial pressure at constant oxygen stoichiometry with $\Delta\delta = 0.05$ (closed symbols) or $\Delta\delta = 0.02$ (open symbols), and for $CeO_{2-\Delta\delta}$ (circles) and $Ce_{1-x}Gd_xO_{2-x/2-\Delta\delta}$ with $x = 0.1$ (squares), $x = 0.2$ (triangles) and $x = 0.3$ (diamonds).

Table 1
Enthalpy (ΔH_R) of reduction for different dopants (Ln) and contents (x) in ceria based solid solutions $Ce_{1-x}Ln_xO_{2-(x/2)-\Delta\delta}$

x	ΔH_R (kJ/mol)	Additive/Reference
0.1	410–420	Gd/this work
	400	Sm/[16]
	438	Gd/[14,15]
0.2	430	Gd/this work
	385	Gd/[14,15]
	385	Sm/[16]
	415	Gd/[20]
	375	Sm/[32]
	350–360	Sm;Gd/[38]

The results in Fig. 2 suggest an inflection for very reducing conditions (dashed lines), especially at the lowest temperatures and for the highest contents of Gd^{3+}. These deviations thus resemble previous observations [15,36,37], and suggest limitations of the ideal model [38]. For example, interactions between oxygen vacancies and the trivalent additive may account for deviations from ideal behaviour [39–41]. In addition, one may expect interactions between polarons and oxygen vacancies in its first coordination in the fluorite structure [17], probably by accommodating stresses caused by relatively large Ce^{3+}.

However, the deviations shown in Fig. 2 may also be due to experimental errors such as differences between the measured emf values and the true condition in the sample, due to slow kinetics, non uniform conditions inside the cell, limitations in gas phase transport of oxygen carrying species, and possibly also electrochemical leakage through the solid electrolyte cell. Such complications are more likely when the cell operates under high cell voltage or at relatively high oxygen pumping currents, i.e., for the highest range of $\Delta\delta$. Thus, we have ignored the results for the highest values of $\Delta\delta$ in Fig. 2, namely above the inflection.

Fig. 4 shows that significant changes in oxygen stoichiometry, and corresponding changes in concentration of ionic and electronic defects, occur under typical fuel conditions containing the reduced and oxidized species (e.g., $H_2 + H_2O$). On assuming equilibrium in the gas phase one easily obtains the relation between the ratio pH_2:pH_2O and the oxygen partial pressure:

$$\frac{pH_2}{pH_2O} = (pO_2)^{-1/2} \exp\left(\frac{\Delta G_{H_2O}}{RT}\right) \tag{15}$$

where ΔG_{H_2O} is free energy of reaction: $H_2 + 1/2O_2 \rightarrow H_2O$.

Such oxygen storage ability and/or substantial changes in concentrations of ionic and electronic species may exert important effects on electrochemical processes taking place at the contact between electrolyte and anode, or when ceria-based materials are used as a component of composite anodes. Note also that the reducibility of CeO_2 is higher than for CGO materials.

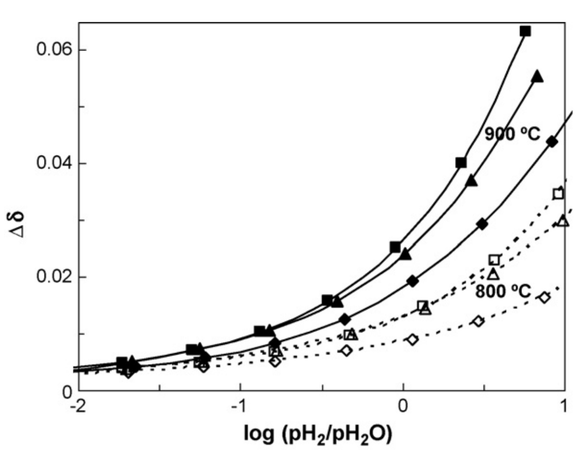

Fig. 4. Dependence of oxygen stoichiometry vs. the H_2:H_2O ratio in fuel atmospheres at 800 °C (open symbols) and 900 °C (closed symbols), for $Ce_{1-x}Gd_xO_{2-x/2-\Delta\delta}$ with $x = 0.1$ (squares), $x = 0.2$ (triangles) and $x = 0.3$ (diamonds).

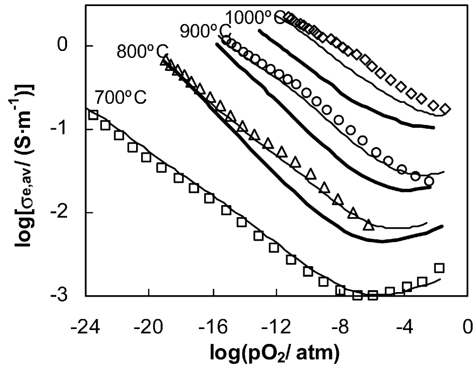

Fig. 5. Average electronic conductivity under 0.21 atm//pO_2 gradients, obtained by the Hebb–Wagner method, $\sigma_{e,av} = (L/S)I/V_0$ for $x = 0.1$ (open symbols), $x = 0.2$ (thin lines) and $x = 0.3$ (thick lines) in $Ce_{1-x}Gd_xO_{2-x/2-\Delta\delta}$.

4. Electronic conductivity

The electronic conductivity was also evaluated by a Hebb–Wagner applied to pellets sintered at 1600 °C during 10 h, with densification in the order of 96%. The average electronic conductivity between air and reducing conditions was then obtained from current–voltage curves (Eq. (3)) and it is shown in Fig. 5. These results clearly show that the onset of electronic current is displaced towards more reducing conditions

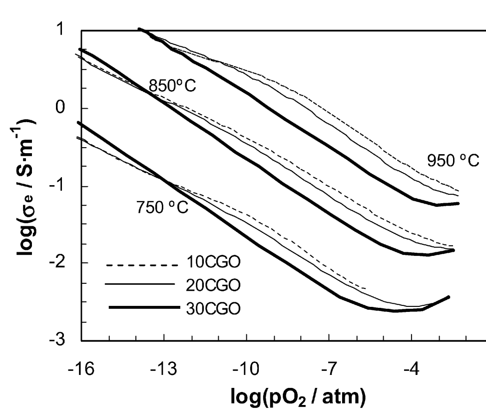

Fig. 6. Electronic conductivity without pO_2 gradient.

Table 2
n-Type electronic conductivity and activation energy at 10^{-10} and 10^{-15} atm

Sample	T (°C)	σ_{hop} (S m^{-1}) $pO_2 = 10^{-10}$ atm	E_{hop} (eV) $pO_2 = 10^{-10}$ atm	σ_{hop} (S m^{-1}) $pO_2 = 10^{-15}$ atm	E_{hop} (eV) $pO_2 = 10^{-15}$ atm
10CGO	1000	–	2.36	–	2.35
	900	10.02×10^{-1}		7.44	
	800	12.65×10^{-2}		11.01×10^{-1}	
	700	10.53×10^{-3}		6.92×10^{-2}	
20CGO	1000	5.97	2.41	53.08	2.48
	900	8.49×10^{-1}		8.09	
	800	9.94×10^{-2}		9.89×10^{-1}	
	700	8.91×10^{-3}		6.25×10^{-2}	
30CGO	1000	3.06	2.30	35.41	2.22
	900	6.15×10^{-1}		8.63	
	800	7.64×10^{-2}		11.04×10^{-1}	
	700	–		–	

when the Gd^{3+}-content increases, indicating a lower electronic contribution under identical reducing conditions.

On differentiating results obtained by the Hebb–Wagner method one also obtained the electronic conductivity at fixed values of pO_2, as shown in Fig. 6, and also in Table 2 (for $pO_2 = 10^{-10}$ and $pO_2 = 10^{-15}$ atm). The temperature dependence at constant pO_2 was used to estimate the activation energy, also shown in Table 2. These values are within the range of 2.2–2.6 eV, as previously reported for different lanthanide-doped ceria [4,25,29,31]. Some discrepancies with the literature data could be due to the fact that the activation energy has often been obtained by extrapolating the electronic conductivity to $pO_2 = 1$ atm, i.e. by several orders of magnitude, which may cause significant deviations.

The similarity between the values of $\Delta H_R/2$ (obtained from Fig. 3) and the activation energy of n-type electronic conductivity indicates that the temperature dependence of electronic transport is mainly related to the reducibility of ceria based materials, with a minor contribution of the temperature dependence of mobility. The polaron mobility (μ_{hop}) was extracted on combining the values of conductivity and oxygen deficiency (Eq. (9)), as follows:

$$\mu_{hop} = \frac{\sigma_{hop}(pO_2, T)}{8e/v_0\, \Delta\delta\,(pO_2, T)} \quad (16)$$

Representative results are shown in Fig. 7. The results for 20% Gd at different temperatures confirm that the mobility is slightly dependent on temperature (Fig. 7a) with activation energy in the range of 0.2–0.6 eV. Though our results of polaron mobility tend to be somewhat lower than other literature data for similar pO_2 (Table 3), the differences can be easily ascribed to experimental errors in the dependence of $\Delta\delta$ versus pO_2, or σ versus pO_2. The results in Fig. 7 also show that the mobility tends to increase with decrease in oxygen deficiency, as reported for CSO [32], and also by other authors [9,11]. This trend may be due to stronger point defect interactions with increasing $\Delta\delta$.

5. Mixed conductivity in prospective fuel cell conditions

One can also examine the effects of electronic conductivity on prospective applications. For example, the values of average electronic and ionic conductivities (σ_I) can be used to obtain the average transport number $t_{e,av} = \sigma_{e,av}/(\sigma_{e,av} + \sigma_I)$ of a solid electrolyte in fuel cell conditions, i.e. under a chemical potential gradient from air to the fuel atmosphere containing $H_2 + H_2O$. For this purpose we have resorted to values of ionic conductivity obtained by impedance spectroscopy in air previously reported [41] and under the assumption that the ionic conductivity is not considerably

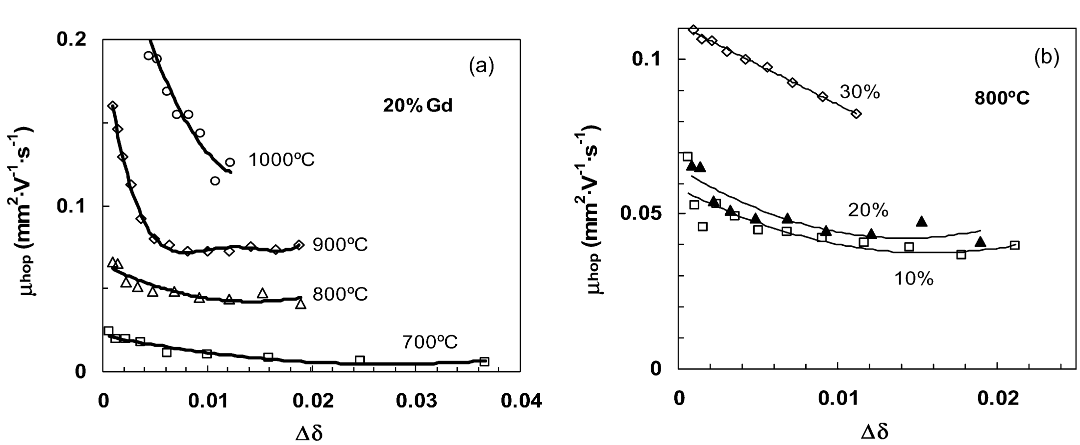

Fig. 7. Polaron mobility results obtained for $Ce_{1-x}Gd_xO_{2-x/2-\Delta\delta}$.

Table 3
Polaron mobility compared with some results extracted from literature

Sample	μ_{hop} ($cm^2\,V^{-1}\,s^{-1}$) ($T=1000\,°C$) ($pO_2 \sim 10^{-12}$ atm)	μ_{hop} ($cm^2\,V^{-1}\,s^{-1}$) ($T=800\,°C$) ($pO_2 \sim 10^{-16}$ atm)	Reference
10CGO	1.0×10^{-3}	0.45×10^{-3}	This work
	3.8×10^{-3}	2.9×10^{-3}	[4]
	5.14×10^{-3}	1.41×10^{-3}	[22]
20CGO	1.3×10^{-3}	0.5×10^{-3}	This work
	3×10^{-3}	2.4×10^{-3}	[4]
	2.91×10^{-3}	1.34×10^{-3}	[22]
30CGO	1.0×10^{-3}	0.97×10^{-3}	This work
CeO_2	8×10^{-3}	4×10^{-3} (725 °C)	[9]
		6.1×10^{-3}	[37]

affected by pO_2. Eq. (15) may then be used to establish the relation between the hydrogen:steam ratio and oxygen partial pressure. Fig. 8 shows results for two representative conditions with gradients corresponding to air/CGO/H_2:H_2O = 1:1 (closed symbols) and air/CGO/H_2:H_2O = 1:10 (open symbols). It is observed that the average electronic transport number increases with temperature and is distinctly higher for the lowest contents of trivalent additive.

The consequences of electronic conductivity can also be analyzed by estimating the effects on the open cell voltage $V_{oc} = V_o(1 - t_{e,av})$, due to the onset of electronic conductivity. For example, Fig. 9 shows the open cell voltage predicted for a cell under a gradient of air/CGO/($H_2 + H_2O$ mixtures). The Nernst potential was calculated on combining Eqs. (1) and (15), and is also shown for comparison. These results confirm that the effect of electronic conductivity on cell voltages is significant for temperatures in the range of 800 °C or higher.

Ceria-based materials are also prospective anode components of solid oxide fuel cells. In this case, the reducibility and onset of mixed ionic-electronic conductivity may contribute to enhance the electrode kinetics. The optimization of ceria-based materials and conditions of operation in solid oxide fuel cells may thus be a compromise between opposite effects of reducibility and electronic conductivity on cell voltage, and electrode kinetics. Representative results of electronic transport number for a fuel condition H_2:H_2O = 1:1 and different values of electrode overpotential are shown in Fig. 10. The anodic overpotential yields

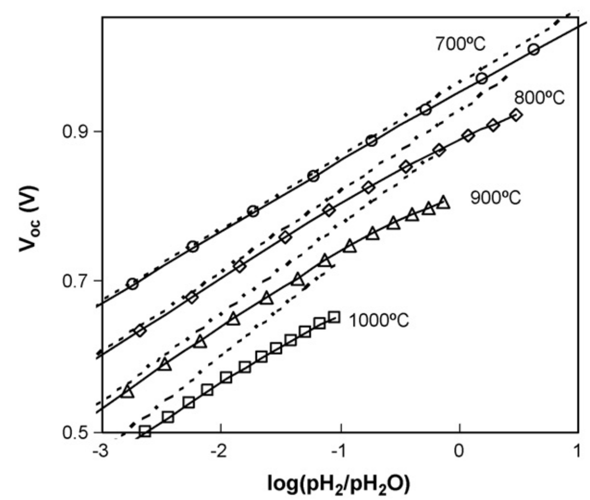

Fig. 9. Estimates of OCV under air//$H_2 + H_2O$ gradients, for $Ce_{0.8}Gd_{0.2}O_{1.9-\Delta\delta}$. The dashed line represents the OCV for an ideal ionic conductor.

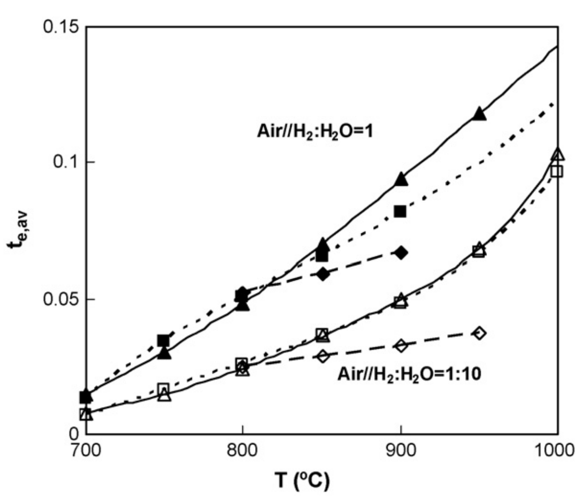

Fig. 8. Temperature dependence of average electronic transport number under Air//H_2:H_2O = 1:1 (closed symbols), and Air//H_2:H_2O = 1:10 (open symbols), for $Ce_{1-x}Gd_xO_{2-x/2-\Delta\delta}$ with $x = 0.1$ (squares), $x = 0.2$ (triangles) and $x = 0.3$ (diamonds).

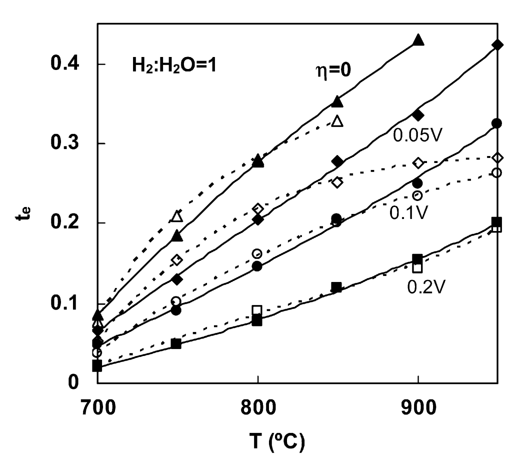

Fig. 10. Estimates of electronic transport numbers of $Ce_{0.8}Gd_{0.2}O_{1.9-\Delta\delta}$ (closed symbols) and $Ce_{0.9}Gd_{0.1}O_{1.95-\Delta\delta}$ (open symbols) under a typical fuel condition H_2:H_2O = 1:1, and with different levels of anodic polarization.

major changes in the electronic transport number, especially at the highest temperatures (Fig. 10). This effect is less pronounced for the lowest contents of Gd ($x = 0.1$), which shows weaker dependence of n-type conductivity on oxygen partial pressure, mainly under very reducing conditions (Fig. 6).

6. Conclusions

We have confirmed that the oxygen deficiency $\Delta\delta$ of $Ce_{1-x}Gd_xO_{2-x/2-\Delta\delta}$ is a guideline to re-examine the role of electronic conductivity in this materials. The changes in oxygen stoichiometry are strongly dependent on temperature and decrease slightly with increasing contents of trivalent additive (Gd^{3+}). Though this is also true for the n-type conductivity under moderately reducing conditions, the trend may be reverted under very reducing conditions, possibly due to significantly higher polaron mobility. We have also evaluated the average electronic conductivity for a solid electrolyte under air/CGO/$H_2 + H_2O$, and combined this information with the ionic conductivity to estimate the effects on open circuit cell voltage. They confirm significant drop in OCV at 800 °C or higher temperatures. The results of electronic and ionic conductivities were also used to evaluate the mixed transport properties of ceria-based materials as prospective anode components, on considering both the dependence on H_2:H_2O ratio and typical values of anodic overpotential.

Acknowledgements

We thank the Spanish Research program (MAT2004-3856), the Canary Islands Government (PI2004/093) and FCT, Portugal (Project POCTI/39381/CTM/2001) by financial support. One of the authors (DP-C) wishes to thank to the Canary Island Government ("Programa de incorporación de Doctores y Tecnólogos a empresas privadas y otras entidades", IDT-TF-06/023) and the OSSEP program (ESF, MCG/OSSEP/2005-60/bol0504). The technical assistance from Luis Hernández is sincerely grateful.

References

[1] H. Yahiro, K. Eguchi, H. Arai, Solid State Ionics 36 (1989) 71.
[2] H. Inaba, H. Tagawa, Solid State Ionics 83 (1996) 1.
[3] G.B. Balaz, R.S. Glass, Solid State Ionics 76 (1995) 155.
[4] B.C.H. Steele, Solid State Ionics 129 (2000) 95.
[5] M. Mogensen, N.M. Sammes, G.A. Tompsett, Solid State Ionics 129 (2000) 63.
[6] J.A. Kilner, B.C.H. Steele, in: T. Sorensen (Ed.), Nonstoichiometric Oxides, Academic Press, New York, 1981, p. 233.
[7] R.N. Blumenthal, R.L. Hofmaier, J. Electrochem. Soc 121 (1974) 126.
[8] R.N. Blumenthal, R.K. Sharma, J. Solid State Chem. 13 (1975) 360.
[9] H.L. Tuller, A.S. Nowick, J. Phys. Chem. Solids 38 (1977) 859.
[10] L. Navarro, F. Marques, J.R. Frade, J. Electrochem. Soc 144 (1) (1997) 267.
[11] M. Mogensen, T. Lindegaard, U.R. Hansen, G. Mogensen, J. Electrochem. Soc. 141 (1994) 2122.
[12] S. Park, J.M. Vohs, R.J. Gorte, Nature 404 (2000) 265.
[13] S. Wang, T. Kato, S. Nagata, T. Honda, T. Kaneko, N. Iwashita, M. Dokiya, J. Electrochem. Soc. 149 (2002) A927.
[14] S.R. Wang, H. Inaba, H. Tagawa, T. Hashimoto, J. Electrochem. Soc. 144 (1997) 4076.
[15] S.R. Wang, H. Inaba, H. Tagawa, M. Dokiya, T. Hashimoto, Solid State Ionics 107 (1998) 73.
[16] T. Kobayashi, S. Wang, M. Dokiya, H. Tagawa, T. Hashimoto, Solid State Ionics 126 (1999) 349.
[17] G. Balducci, M.S. Islam, J. Kaspar, P. Fornaseiro, M. Graziani, Chem. Mater. 15 (2003) 3781.
[18] B. Zachau-Christiansen, T. Jacobsen, S. Skaarup, Solid State Ionics 86 (1996) 725.
[19] I. Yasuda, M. Hishinuma, in: T.A. Ramanarayanan, W. Worrel, H.L. Tuller, A.C. Khandkar, M. Mogensen, W. Gopel (Eds.), Ionic and Mixed Conducting Ceramics III, vol. 97(24), Electrochem. Soc. Proc., 1998, p. 178.
[20] T. Kudo, H. Obayashi, J. Electrochem. Soc. 123 (1976) 415.
[21] H.L. Tuller, in: T. Sorensen (Ed.), Nonstoichiometric Oxides, Academic Press, New York, 1981, p. 271.
[22] S. Wang, T. Kobayashi, M. Dokiya, T. Hashimoto, J. Electrochem. Soc. 147 (10) (2000) 3606.
[23] M.H. Hebb, J. Chem. Phys. 20 (1952) 185.
[24] C. Wagner, Proceedings of the Seventh Meeting of the International Committee on Electrochemical Thermodynamics and Kinetics, Lindau, Butterworths Scientific Publication, London, 1957, p. 361.
[25] S. Lubke, H.D. Wiemhofer, Solid State Ionics 117 (1999) 229.
[26] Y. Xiong, K. Yamaji, N. Sakai, H. Negishi, T. Horita, H. Yokokawa, J. Electrochem. Soc 148 (12) (2001) E489.
[27] Y. Xiong, K. Yamaji, T. Horita, N. Sakai, H. Yokokawa, J. Electrochem. Soc. 149 (11) (2002) E450.
[28] D.P. Fagg, J.C.C. Abrantes, D. Pérez-Coll, P. Núñez, V.V. Kharton, J.R. Frade, Electrochim. Acta 48 (2003) 1023.
[29] D. Pérez-Coll, D. Marrero-López, P. Núñez, J.C.C. Abrantes, J.R. Frade, J. Solid State Electrochem. 8 (9) (2004) 644.
[30] D. Pérez-Coll, P. Núñez, J.C.C. Abrantes, D.P. Fagg, V.V. Kharton, J.R. Frade, Solid State Ionics 176 (2005) 2799.
[31] Y. Xiong, K. Yamaji, T. Horita, N. Sakai, H. Yokokawa, J. Electrochem. Soc. 151 (3) (2004) A407.
[32] J.C.C. Abrantes, D. Pérez-Coll, P. Núñez, J.R. Frade, Electrochim. Acta 48 (2003) 2761.
[33] D. Pérez-Coll, P. Núñez, J.R. Frade, J.C.C. Abrantes, Electrochim. Acta 48 (2003) 1551.
[34] A.A.L. Ferreira, J.C.C. Abrantes, J.R. Jurado, J.R. Frade, Solid State Ionics 135 (2000) 761.
[35] V.N. Tikhonovich, E.N. Naumovich, V.V. Kharton, A.A. Yaremchenko, A.V. Kovalevsky, A.A. Vecher, Electrochim. Acta 47 (2002) 3957.
[36] I. Riess, H. Janczikowski, J. Nolting, J. Appl. Phys. 61 (1987) 4931.
[37] M.A. Panhans, R.N. Blumenthal, Solid State Ionics 60 (1993) 279.
[38] D. Schneider, M. Godickemeier, L.J. Gauckler, J. Electroceram. 1 (1997) 165.
[39] K. Huang, M. Feng, J.B. Goodenough, J. Am. Ceram. Soc. 81 (1998) 357.
[40] G.B. Jung, T.J. Huang, C.L. Chang, J. Solid State Electrochem. 6 (2002) 225.
[41] D. Pérez-Coll, P. Núñez, J.C. Ruiz-Morales, J. Peña-Martínez, J.R. Frade, Electrochim. Acta 52 (2007) 2001.